Metal-Insulator Transitions and Realistic Modelling of Correlated Electron Systems

Georg Keller[1], Dieter Vollhardt[1], Karsten Held[1,2], Volker Eyert[1], and Vladimir I. Anisimov[3]

[1] Center for Electronic Correlations and Magnetism, Theoretical Physics III
Institute for Physics, University of Augsburg
86135 Augsburg, Germany
[2] Physics Department, Princeton University
Princeton, NJ 08544, USA
[3] Institute of Metal Physics
Ekaterinburg, GSP-170, Russia

1 Introduction

The calculation of physical properties of electronic systems by controlled approximations is one of the most important challenges of modern theoretical solid state physics. In particular, the physics of transition metal oxides – a singularly important group of materials both from the point of view of fundamental research and technological applications – may only be understood by explicit consideration of the strong effective interaction between the conduction electrons in these systems. The investigation of electronic many-particle systems is made especially complicated by quantum statistics, and by the fact that the phenomena of interest (e.g., metal insulator transitions and ferromagnetism) usually require the application of non-perturbative theoretical techniques.

One of the most famous examples of a cooperative electronic phenomenon of this type is the transition between a paramagnetic metal and a paramagnetic insulator induced by the Coulomb interaction between the electrons, referred to as Mott-Hubbard metal-insulator transition. The question concerning the nature of this transition poses one of the fundamental theoretical problems in condensed matter physics [1, 2]. Correlation-induced metal-insulator transitions (MIT) are found, for example, in transition metal oxides with partially filled bands near the Fermi level. For such systems band theory typically predicts metallic behavior. The most famous example is V_2O_3 doped with Cr [3, 4, 5]; see Fig. 1.

While at low temperatures V_2O_3 is an antiferromagnetic insulator with monoclinic crystal symmetry, it has a corundum structure with a small trigonal distortion in the high-temperature paramagnetic phase. All transitions shown in the phase diagram (Fig. 1) are of first order. In the case of the transitions from the high-temperature paramagnetic phases into the low-

temperature antiferromagnetic phase this is naturally explained by the fact that the transition is accompanied by a change in crystal symmetry. By contrast, the crystal symmetry across the MIT in the paramagnetic phase remains intact, since only the ratio of the c/a axes changes discontinuously. This is usually taken as an indication for the predominantly electronic origin of this MIT, caused by strong correlations.

In the last decade, a new approach for treating electronic lattice models, the dynamical mean-field theory (DMFT), has led to new analytical and numerical opportunities to study correlated electronic systems [6,7]. This theory, introduced by the work of Metzner and Vollhardt in 1989, is exact in the limit of infinite dimensions ($d = \infty$) [8]. In this limit, the problem is reduced to a single-impurity Anderson model with self consistency condition [9,10,11], allowing for a solution by quantum Monte-Carlo (QMC) simulations without a sign problem for one-band models (for multi-band models, see Ref. [12]),i.e. down to temperatures $T \sim 10^{-2}W$ (W: bandwidth).

Recently, the LDA+DMFT, a new computation scheme that merges electronic band structure calculations and the dynamical mean field theory, was developed [13,14,15,16]. Starting from conventional band structure calculations in the local density approximation (LDA) the correlations are taken into account by a Hubbard interaction term and a Hund's rule coupling term. The resulting DMFT equations are solved numerically with a parallelized auxiliary-field quantum Monte-Carlo algorithm. This scheme makes possible the investigation of real systems close to a Mott-Hubbard transition such as the MIT in V_2O_3 discussed above. In this paper, results on

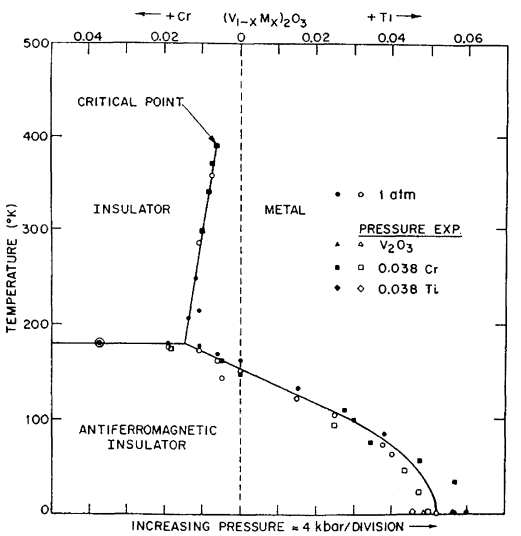

Fig. 1. Phase Diagram of V_2O_3 doped with Cr or Ti (temperature versus external pressure); from [4].

the correlation-induced metal-insulator transition and dynamic properties of multi-band Hubbard-type models at low temperatures obtained within the DMFT are presented. Calculations at experimentally relevant temperatures were made possible by the increased computer power of the Hitachi SR8000-F1.

2 Method and algorithm

2.1 General remarks

Although the one band Hubbard model is able to explain certain basic features of the Mott-Hubbard MIT and the phase diagram of V_2O_3, it cannot explain the physics of that material in any detail. Clearly, a realistic theory of V_2O_3 must take into account the complicated electronic structure of this system. In the high-temperature paramagnetic phase V_2O_3 has an electronic structure with a $3d^2$ V^{3+} state, where the two e_g-orbitals are empty and the three t_{2g}-orbitals are filled with two electrons. A small trigonal distortion lifts the triple degeneracy of the t_{2g}-orbitals, resulting in one non-degenerate a_{1g}-orbital and two degenerate e_g^π orbitals.

For the investigation of such realistic multi-band systems near a Mott-Hubbard MIT, the best available method is LDA+DMFT which has been developed recently [13,14,15,16,17,18].

In the LDA+DMFT approach the LDA band structure, expressed by a one-particle Hamiltonian H^0_{LDA}, is supplemented with the local Coulomb repulsion U and Hund's rule exchange J:

$$\hat{H} = \hat{H}^0_{\mathrm{LDA}} + U \sum_m \sum_i \hat{n}_{im\uparrow}\hat{n}_{im\downarrow} + \sum_{i,m\neq\tilde{m},\sigma,\tilde{\sigma}} (V - \delta_{\sigma\tilde{\sigma}} J)\, \hat{n}_{im\sigma}\hat{n}_{i\tilde{m}\tilde{\sigma}}. \quad (1)$$

Here, i denotes the lattice site; m and $\tilde{m}$ enumerate the three interacting t_{2g} orbitals. The interaction parameters are related by $V = U - 2J$ which holds exactly for degenerate orbitals and is a good approximation for the t_{2g} orbitals. Furthermore, since the t_{2g} bands at the Fermi energy are rather well separated from all other bands we restrict the calculation to these bands (for details of the computational scheme see [16,17]). With this restriction only the LDA DOS of the three t_{2g} bands enter the LDA+DMFT calculation [17]. The LDA-calculated value of the Coulomb repulsion U has a typical uncertainty of at least 0.5 eV [16]. For this reason, we adjust U to yield a metal-insulator transition with Cr doping. *A posteriori*, we can compare whether the adjusted value is in the range of values obtained from a constrained LDA calculation.

2.2 Description of the algorithm

During the last ten years, DMFT has proved to be a successful approach to investigate strongly correlated systems with local Coulomb interactions

[7]. It becomes exact in the limit of high lattice coordination numbers [8, 19] and preserves the dynamics of local interactions. Hence, it represents a *dynamical* mean-field approximation. In this non-perturbative approach the lattice problem is mapped onto an effective single-site problem which has to be determined self-consistently together with the **k**-integrated Dyson equation connecting the self energy Σ and the Green function G at frequency ω. Within the LDA+DMFT scheme this implies:

$$G_{qlm,q'l'm'}(\omega) = \frac{1}{V_B} \int d^3k \left(\left[\omega 1 + \mu 1 - H^0_{\mathrm{LDA}}(\mathbf{k}) - \Sigma(\omega) \right]^{-1} \right)_{qlm,q'l'm'} . \quad (2)$$

Here, 1 is the unit matrix, μ the chemical potential, $H^0_{\mathrm{LDA}}(\mathbf{k})$ the LDA Hamiltonian derived in a LMTO-basis, $\Sigma(\omega)$ denotes the self-energy matrix which is non-zero only between the interacting orbitals, $[...]^{-1}$ implies the inversion of the matrix with elements n $(=qlm)$, $n'(=q'l'm')$, and the integration extends over the Brillouin zone with volume V_B.

The DMFT single-site problem depends on $\mathcal{G}(\omega)^{-1} = G(\omega)^{-1} + \Sigma(\omega)$ and is equivalent [11, 9] to an Anderson impurity model if its hybridization $\Delta(\omega)$ satisfies $\mathcal{G}^{-1}(\omega) = \omega - \int d\omega' \Delta(\omega')/(\omega - \omega')$. The local one-particle Green function at a Matsubara frequency $i\omega_\nu = i(2\nu + 1)\pi/\beta$ (β: inverse temperature), orbital index m ($l = l_d$, $q = q_d$), and spin σ is given by the following functional integral over Grassmann variables ψ and ψ^*:

$$G^\sigma_{\nu m} = -\frac{1}{\mathcal{Z}} \int \mathcal{D}[\psi]\mathcal{D}[\psi^*] \psi^\sigma_{\nu m} \psi^{\sigma *}_{\nu m} e^{\mathcal{A}[\psi, \psi^*, \mathcal{G}^{-1}]} . \quad (3)$$

Here, $\mathcal{Z} = \int \mathcal{D}[\psi]\mathcal{D}[\psi^*] \exp(\mathcal{A}[\psi, \psi^*, \mathcal{G}^{-1}])$ is the partition function and the single-site action $\mathcal{A}$ has the form (the interaction part of $\mathcal{A}$ is in terms of the "imaginary time" τ, i.e., the Fourier transform of ω_ν)

$$\begin{aligned} \mathcal{A}[\psi, \psi^*, \mathcal{G}^{-1}] &= \sum_{\nu,\sigma,m} \psi^{\sigma *}_{\nu m} (\mathcal{G}^\sigma_{\nu m})^{-1} \psi^\sigma_{\nu m} \\ &- \frac{1}{2} {\sum_{m\sigma,m\sigma'}}' U^{\sigma\sigma'}_{mm'} \int_0^\beta d\tau \, \psi^{\sigma *}_m(\tau) \psi^\sigma_m(\tau) \psi^{\sigma' *}_{m'}(\tau) \psi^{\sigma'}_{m'}(\tau) \\ &+ \frac{1}{2} {\sum_{m\sigma,m}}' J_{mm'} \int_0^\beta d\tau \, \psi^{\sigma *}_m(\tau) \psi^{\bar{\sigma}}_m(\tau) \psi^{\bar{\sigma} *}_{m'}(\tau) \psi^\sigma_{m'}(\tau) \ . \end{aligned} \quad (4)$$

This single-site problem (3) has to be solved self-consistently together with the **k**-integrated Dyson equation (2) to obtain the DMFT solution of a given problem.

The QMC algorithm by Hirsch and Fye [20] is a well established method to find a numerically exact solution for the Anderson impurity model and allows one to calculate the impurity Green function G at a given $\mathcal{G}^{-1}$ as well

as correlation functions. In essence, the QMC technique maps the interacting electron problem (3) onto a sum of non-interacting problems where the single particle moves in a fluctuating, time-dependent field and evaluates this sum by Monte Carlo sampling. To this end, the imaginary time interval $[0, \beta]$ of the functional integral equation (3) is discretized into Λ steps of size $\Delta\tau = \beta/\Lambda$, yielding support points $\tau_l = l\Delta\tau$ with $l = 1 \ldots \Lambda$. Using this Trotter discretization, the integral $\int_0^\beta d\tau$ is transformed to the sum $\sum_{l=1}^{\Lambda} \Delta\tau$ and the exponential terms in (3) can be separated via the Trotter-Suzuki formula [21], which is exact in the limit $\Delta\tau \to 0$. The single site action $\mathcal{A}$ of (4) can now be written in the discrete, imaginary time as

$$\mathcal{A}[\psi, \psi^*, \mathcal{G}^{-1}] = \Delta\tau^2 \sum_{\sigma\, m\, l,l'=0}^{\Lambda-1} {\psi_{ml}^{\sigma}}^* {\mathcal{G}_m^{\sigma}}^{-1}(l\Delta\tau - l'\Delta\tau)\psi_{ml'}^{\sigma}$$
$$-\frac{1}{2}\Delta\tau {\sum_{m\sigma,m'\sigma'}}' U_{mm'}^{\sigma\sigma'} \sum_{l=0}^{\Lambda-1} {\psi_{ml}^{\sigma}}^* \psi_{ml}^{\sigma} {\psi_{m'l}^{\sigma'}}^* \psi_{m'l}^{\sigma'}, \qquad (5)$$

where the first term was Fourier-transformed from Matsubara frequencies to imaginary time. In a second step, the $M(2M-1)$ interaction terms in the single site action $\mathcal{A}$ are decoupled by introducing a classical auxiliary field $s_{lmm'}^{\sigma\sigma'}$:

$$\exp\left\{\frac{\Delta\tau}{2} U_{mm'}^{\sigma\sigma'} ({\psi_{ml}^{\sigma}}^* \psi_{ml}^{\sigma} - {\psi_{m'l}^{\sigma'}}^* \psi_{m'l}^{\sigma'})^2\right\} =$$
$$\frac{1}{2} \sum_{s_{lmm'}^{\sigma\sigma'}=\pm 1} \exp\left\{\Delta\tau \lambda_{lmm'}^{\sigma\sigma'} s_{lmm'}^{\sigma\sigma'} ({\psi_{ml}^{\sigma}}^* \psi_{ml}^{\sigma} - {\psi_{m'l}^{\sigma'}}^* \psi_{m'l}^{\sigma'})\right\}, \qquad (6)$$

where $\cosh(\lambda_{lmm'}^{\sigma\sigma'}) = \exp(\Delta\tau U_{mm'}^{\sigma\sigma'}/2)$ and M is the number of interacting orbitals. This so-called discrete Hirsch-Fye-Hubbard-Stratonovich transformation can be applied to the Coulomb repulsion as well as the Z-component of Hund's rule coupling [12]. It replaces the interacting system by a sum of $\Lambda M(2M-1)$ auxiliary fields $s_{lmm'}^{\sigma\sigma'}$. The functional integral can now be solved by a simple Gauss integration because the Fermion operators only enter quadratically, i.e., for a given configuration $\mathbf{s} = \{s_{lmm'}^{\sigma\sigma'}\}$ of the auxiliary fields the system is non-interacting. The quantum mechanical problem is then reduced to a matrix problem

$$G_{\tilde{m}l_1l_2}^{\tilde{\sigma}} = \frac{1}{\mathcal{Z}} \frac{1}{2} \sum_{l} {\sum_{m'\sigma',m''\sigma''}}' \sum_{s_{lm''m'}^{\sigma''\sigma'}=\pm 1} \left[(M_{\tilde{m}}^{\tilde{\sigma}\mathbf{s}})^{-1}\right]_{l_1l_2} \prod_{m\sigma} \det \mathbf{M}_m^{\sigma\mathbf{s}} \qquad (7)$$

with the partition function $\mathcal{Z}$, the matrix

$$\mathbf{M}_{\tilde{m}}^{\tilde{\sigma}\mathbf{s}} = \Delta\tau^2 [\mathbf{G}_m^{\sigma\,-1} + \Sigma_m^{\sigma}] e^{-\tilde{\lambda}_m^{\sigma\mathbf{s}}} + \mathbf{1} - e^{-\tilde{\lambda}_m^{\sigma\mathbf{s}}} \qquad (8)$$

and the elements of the matrix $\tilde{\lambda}_m^{\sigma\mathbf{s}}$

$$\tilde{\lambda}_{mll'}^{\sigma\mathbf{s}} = -\delta_{ll'} \sum_{m'\sigma'} \lambda_{mm'}^{\sigma\sigma'} \tilde{\sigma}_{mm'}^{\sigma\sigma'} s_{lmm'}^{\sigma\sigma'}. \tag{9}$$

Here $\tilde{\sigma}_{mm'}^{\sigma\sigma'} = 2\Theta(\sigma' - \sigma + \delta_{\sigma\sigma'}[m' - m] - 1)$ changes sign if $(m\sigma)$ and $(m'\sigma')$ are exchanged. For more details, e.g., for a derivation of (8) for the matrix $\mathbf{M}$, see [20, 9, 7].

Since the sum in (7) consists of $2^{\Lambda M(2M-1)}$ addends, a complete summation for large Λ is computationally impossible. Therefore the Monte Carlo method, which is often an efficient way to calculate high-dimensional sums and integrals, is employed for importance sampling of (7). Further details of the employed QMC algorithm can be found in [18].

Using a Markov process and single spin-flips in the auxiliary fields, the computational cost of the algorithm in leading order of Λ is

$$2aM(2M-1)\Lambda^3 \times \text{number of MC-sweeps}, \tag{10}$$

where a is the acceptance rate for a single spin-flip.

The advantage of the QMC method is that it is (numerically) exact. It allows one to calculate the one-particle Green function as well as two-particle (or higher) Green functions. On present workstations the QMC approach is able to deal with up to three *interacting* orbitals at temperatures of about 700 K. Very low temperatures are not accessible because the numerical effort grows like $\Lambda^3 \propto 1/T^3$. Since the QMC approach calculates $G(\tau)$ or $G(i\omega_n)$ with a statistical error, it also requires the maximum entropy method [22] to obtain the Green function $G(\omega)$ at real (physical) frequencies ω.

3 Results

In a first step, LDA calculations were performed for paramagnetic *metallic* V_2O_3 and paramagnetic *insulating* $(V_{0.962}Cr_{0.038})_2O_3$, respectively [23]. The LDA results for corundum V_2O_3 and $(V_{0.962}Cr_{0.038})_2O_3$ are very similar. In particular, the changes in crystal and electronic structure occuring at the transition are insufficiently reflected by the LDA calculations and the experimentally observed insulating gap is *missing* in the LDA DOS. It is generally believed that this insulating gap is due to strong Coulomb interactions which are not adequately accounted for by the LDA. This is where our LDA+DMFT(QMC) scheme sets in. Using this approach we can show explicitly that the insulating gap is indeed caused by electronic correlations.

The spectra obtained by LDA+DMFT(QMC) imply that the critical value of U for the MIT is about 5 eV [23]. Indeed, at $U = 4.5$ eV one observes pronounced quasiparticle peaks at the Fermi energy, i.e., characteristic metallic behavior, even for the crystal structure of $(V_{0.962}Cr_{0.038})_2O_3$, while at

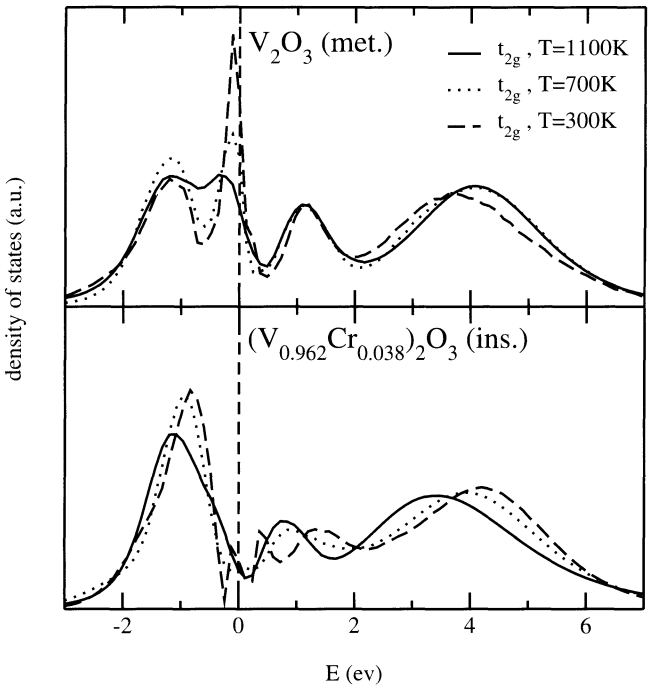

Fig. 2. LDA+DMFT(QMC) spectrum for metallic V_2O_3 and insulating $(V_{0.962}Cr_{0.038})_2O_3$ for $U = 5$ eV at $T = 1100$ K, $T = 700$ K and $T = 300$ K

$U = 5.5$ eV the form of the calculated spectral function is typical for an insulator for both sets of crystal structure parameters.

Whereas for the computations at $T = 1100$ K (which were done on a workstation), we only observe metallic-like and insulating-like behavior, with a rapid but smooth crossover between these two phases, the calculations done on the Hitachi SR8000-F1 at lower temperatures (Fig. 2) show more pronounced differences between the metallic and insulating phase; the smooth crossover is replaced by a sharp first order metal-insulator transition [24,25].

To compare with the photoemission spectrum of V_2O_3 by Schramme et al. [26] and Kim et al. [27] the LDA+DMFT(QMC) spectra are multiplied with the Fermi function at $T = 1100$ K and Gauss-broadened by 0.05 eV to account for the experimental resolution. In contrast to the LDA results, the theoretical results [23] for $U = 5$ eV are seen to be in good agreement with experiment (Fig. 3). We also note that the DOS is highly asymmetric with respect to the Fermi energy due to the orbital degrees of freedom. This is in striking contrast to the result obtained with a one-band model. The comparison between our results, the data of Müller et al. [28] obtained by X-ray absorption measurements, and LDA in Fig. 4 shows that, in contrast with LDA, our results not only describe the different bandwidths above *and*

below the Fermi energy (≈ 6 eV and $\approx 2-3$ eV, respectively) correctly, but even resolve the two-peak structure above the Fermi energy.

Particularly interesting are the spin and the orbital degrees of freedom in V_2O_3. We find (not shown) that for $U \gtrsim 3$ eV the squared local magnetic moment $\langle m_z^2 \rangle$ saturates at a value of 4, i.e., there are *two* electrons with the same spin direction in the (a_{1g}, e_{g1}^{π}, e_{g2}^{π}) orbitals [23]. Thus, we conclude that the spin state of V_2O_3 is $S = 1$ throughout the Mott-Hubbard transition region. Our $S = 1$ result agrees with the measurements of Park et al. [29] and also with the data for the high-temperature susceptibility. Thus LDA+DMFT(QMC) provides a remarkably accurate microscopic theory of the strongly correlated electrons in the paramagnetic phase of V_2O_3 [23].

4 Summary

Applying the newly developed LDA+DMFT(QMC) scheme, which merges the conventional local density approximation (LDA) with DMFT in combination with QMC, to investigate the paramagnetic phase of V_2O_3 we find remarkable agreement with recent experiments. Indeed, LDA+DMFT(QMC) turns out to be a workable computational scheme which provides, at last, a powerful tool for future *ab initio* investigations of real materials with strong electronic correlations.

Future investigations will have to clarify the origin of the discontinuous lattice distortion at the first-order metal-insulator transition which leaves

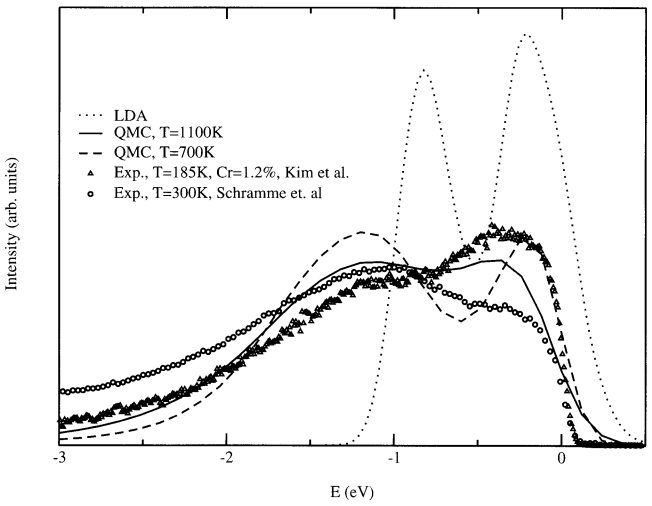

Fig. 3. Comparison of the LDA+DMFT(QMC) spectra [23] with the LDA spectrum and the photoemission experiments on metallic V_2O_3 by Schramme et al. [26](pure sample) and Kim et al. (Cr doped sample).

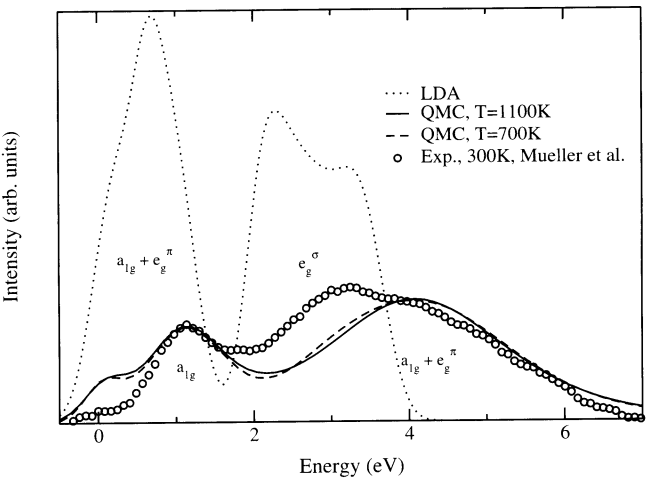

Fig. 4. Comparison of the LDA and LDA+DMFT(QMC) spectra at $T = 0.1$ eV (Gaussian broadened with 0.2 eV) [23] with the X -ray absorption data of Müller et al. [28].

the lattice symmetry unchanged. In particular, the metal-insulator transition might be the driving force behind the lattice distortion by causing a thermodynamic instability with respect to changes of the lattice volume and distortions. Such investigations at experimentally relevant temperatures are only possible on supercomputers like the Hitachi SR8000-F1. Eventually truly realistic investigations of transition metals and their oxides will require a genuine fusion of LDA with DMFT and the inclusion of all relevant electronic bands. As discussed above a larger number of bands and lower temperatures imply an enormous increase of numerical effort. This shows that substantial progress in the modelling of correlated electronic materials will only be possible with much faster computers.

We gratefully acknowledge support by the Leibniz-Rechenzentrum through HLRB-project h0531 and by the Deutsche Forschungsgemeinschaft through Sonderforschungsbereich 484.

References

1. N. F. Mott, Rev. Mod. Phys. **40**, 677 (1968); *Metal-Insulator Transitions* (Taylor & Francis, London, 1990).
2. F. Gebhard, *The Mott Metal-Insulator Transition* (Springer, Berlin, 1997).
3. D. B. McWhan and J. P. Remeika, Phys. Rev. **B2**, 3734 (1970).
4. D. B. McWhan et al., Phys. Rev. **B7**, 1920 (1973).
5. T. M. Rice and D. B. McWhan, IBM J. Res. Develop. 251 (May 1970).
6. D. Vollhardt, Investigation of correlated electron systems using the limit of high dimensions, in *Correlated Electron Systems*, Hrsg.: V. J. Emery, World Scientific, Singapore, 1993.

7. A. Georges, G. Kotliar, W. Krauth und M. Rozenberg, Rev. Mod. Phys. **68**, 13 (1996).
8. W. Metzner und D. Vollhardt, Phys. Rev. Lett. **62**, 324 (1989).
9. M. Jarrell, Phys. Rev. Lett. **69**, 168 (1992).
10. M. Jarrell und T. Pruschke, Z. Phys. B **90**, 187 (1993).
11. A. Georges und G. Kotliar, Phys. Rev. B **45**, 6479 (1992).
12. One limitation of QMC is that it is very difficult to deal with the spin-flip term of the Hund's rule coupling because of a "minus-sign problem" which arises in a Hubbard-Stratonovich decoupling of this spin-flip term, see K. Held, Ph.D. thesis Universität Augsburg 1999 (Shaker Verlag, Aachen, 1999).
13. V. I. Anisimov, A. I. Poteryaev, M. A. Korotin, A. O. Anokhin, and G. Kotliar, J. Phys.: Cond. Matt. **9**, 7359 (1997).
14. A. I. Lichtenstein and M. I. Katsnelson, Phys. Rev. B **57**, 6884 (1998).
15. M. B. Zölfl, Th. Pruschke, J. Keller, A. I. Poteryaev, I. A. Nekrasov, and V. I. Anisimov, Phys. Rev. B **61**, 12810 (2000).
16. I. A. Nekrasov, K. Held, N. Blümer, A. I. Poteryaev, V. I. Anisimov, and D. Vollhardt, Euro Phys. J. B **18**, 55 (2000).
17. K. Held, I. A. Nekrasov, N. Blümer, V. I. Anisimov, and D. Vollhardt, Int. J. Mod. Phys. B **15**, 2611 (2001).
18. For an introduction into LDA+DMFT, see K. Held, I.A. Nekrasov, G. Keller, V. Eyert, N. Blümer, A.K. McMahan, R.T. Scalettar, T. Pruschke, V.I. Anisimov, D. Vollhardt, Quantum Simulations of Complex Many-Body Systems: From Theory to Algorithms, eds. J. Grotendorst, D. Marx and A. Muramatsu, NIC Series Vol. 10 (NIC Directors, Forschungszentrum J?lich, 2002), p. 175.
19. E. Müller-Hartmann, Z. Phys. B **74**, 507 (1989); ibid. B **76**, 211 (1989).
20. J. E. Hirsch and R. M. Fye, Phys. Rev. Lett. **56**, 2521 (1986); M. Rozenberg, X. Y. Zhang, and G. Kotliar, Phys. Rev. Lett. **69**, 1236 (1992); A. Georges and W. Krauth, Phys. Rev. Lett. **69**, 1240 (1992); M. Jarrell, in *Numerical Methods for Lattice Quantum Many-Body Problems*, edited by D. Scalapino, Addison Wesley, 1997.
21. M. Suzuki, Prog. Theor. Phys. **56**, 1454 (1976)
22. M. Jarrell and J. E. Gubernatis, Physics Reports **269**, 133 (1996).
23. K. Held, G. Keller, V. Eyert, D. Vollhardt, and V. I. Anisimov, Phys. Rev. Lett. **86**, 5345 (2001).
24. M. J. Rozenberg, Phys. Rev. B **55**, R4855 (1997).
25. G. Moeller, Q. Si, G. Kotliar, M. J. Rozenberg, and D. S. Fisher, Phys. Rev. Lett. **74**, 2082 (1995); J. Schlipf, M. Jarrell, P. G. J. van Dongen, N. Blümer, S. Kehrein, Th. Pruschke, and D. Vollhardt, Phys. Rev. Lett. **82**, 4890 (1999); M. J. Rozenberg, R. Chitra and G. Kotliar, Phys. Rev. Lett. **83**, 3498 (1999); R. Bulla, Phys. Rev. Lett. **83**, 136 (1999).
26. M. Schramme, Ph.D. thesis, Universität Augsburg, 2000; M. Schramme et al. (unpublished).
27. H.-D. Kim, J.-H. Park, J. W. Allen, A. Sekiyama, A. Yamasaki, K. Kadono, S. Suga, Y. Saitoh, T. Muro, and P. Metcalf, cond-mat/0108044.
28. O. Müller, J. P. Urbach, E. Goering, T. Weber, R. Barth, H. Schuler, M. Klemm, S. Horn, and M. L. denBoer, Phys. Rev. B **56**, 15056 (1997).
29. J.-H. Park, L.H. Tjeng, A. Tanaka, J.W. Allen, C.T. Chen, P. Metcalf, J.M. Honig, F.M.F. de Groot, and S.A. Sawatzky, Phys. Rev. B **61**, 11 506 (2000).